JOURNAL OF SCIENCE AND TECHNOLOGY
ISSN: 2229-8460 e-ISSN: 2600-7924

JST

Vol. 17 No. 2 (2025) 166-177
https://publisher.uthm.edu.my/ojs/index.php/jst

Synthesis and Characterization of As-Synthesized Co-deposited PbS/ZnS Thin Films Prepared by SILAR Technique

Ibrahim B. Omoteji[1], Francis O. Omoniyi[1]*, Olayinka A. Babalola[1], Thomas I. Imalerio[1]

[1] *Physics Advanced Research Center,*
SHEDA Science and Technology Center, Kwali, 904105, NIGERIA

*Corresponding Author: omoniyifrancis@gmail.com
DOI: https://doi.org/10.30880/jst.2025.17.02.013

Article Info

Received: 26 August 2025
Accepted: 25 November 2025
Available online: 30 December 2025

Keywords

PbS/ZnS, SILAR, deposition cycles, optoelectronics

Abstract

Thin-film semiconductors are widely studied for their applications in various optoelectronic devices. PbS and ZnS are useful semiconductors for various optoelectronic applications, with PbS having low energy bandgap while ZnS has wide energy bandgap. In this paper, we investigate the structural, morphological, optical and electrical properties of the as-synthesized PbS/ZnS films and evaluate their potential in optoelectronic applications. PbS/ZnS thin film was synthesized using the Successive Ionic Layer Adsorption and Reaction (SILAR) method, by varying deposition cycles without post-deposition annealing. The X-ray diffraction (XRD) peaks confirmed the presence of cubic phases of PbS and ZnS with increasing crystallinity at higher SILAR cycles. Scanning electron microscopy (SEM) revealed enhanced surface coverage and grain growth with increased cycles while energy disperse X-ray spectroscopy (EDS) verified the presence of Pb, Zn and S. Optical bandgap energies ranged from 1.43 eV to 2.82 eV, which is attributed to changes in film thickness and composition**.** Hall Effect showed n-type conductivity with varying carrier concentration and mobility. These results highlighted the tunability of PbS/ZnS thin films via SILAR cycles, making them promising for application in solar cells and photodetectors.

1. Introduction

Lead Sulphide (PbS) and Zinc Sulphide (ZnS) thin films are widely studied for their tunable optoelectronic properties, making them suitable for applications in solar cells, sensors and light emitting diodes. PbS, a narrow-band gap semiconductor 0.4 eV, is ideal for window layers and UV optoelectronics. On the other hand, ZnS has wide band gap of either about 3.6 eV (Zincblende) or about 3.91 eV (Wurtzite). Co-deposition of PbS and ZnS combines their complementary properties, enhancing device performance through bandgap engineering and improved charge transport [1-3]. Various techniques, including chemical vapour deposition, magnetron sputtering, Successive Ionic Layer Adsorption and Reaction **(**SILAR), thermal evaporation and spray pyrolysis have been used to deposit PbS and ZnS thin films. However, SILAR method stands out for its simplicity, cost effectiveness and ability to control thin film thickness at nanoscale without requiring high vacuum and high temperature [4-6]. SILAR enables precise co-deposition of PbS and ZnS, allowing tailored structural and optical properties, by adjusting deposition cycles [7]. Previous research has extensively explored how deposition techniques influenced deposited material properties [8], which are often significantly influenced by the

materials at the interface. They can promote nanostructured nucleation and enhance growth. However, most of the existing deposition methods lack precise control of film thickness at nanoscale [9], except for the Atomic Layer Deposition method [10], which lacks both simplicity and cheap cost like SILAR method.

This study investigates the synthesis of PbS/ZnS thin films via SILAR without post-deposition annealing, which is a less explored approach that preserves the as-synthesized properties of the films. By varying the deposition cycles (4 to 14), we aim to elucidate the impact on structural, morphological, optical and electrical properties of thin films and thus, assess their suitability for optoelectronics applications [11, 12]. This work thus builds on recent advances in SILAR deposited and chalcogenide films.

2. Materials and Methods

2.1 Materials

The synthesis of PbS/ZnS co-deposited thin films using the SILAR technique was achieved, using 0.1 M solutions of lead nitrate and zinc chloride serving as sources of Pb^{2+} and Zn^{2+}, respectively, and a 0.05 M sodium sulfide solution providing S^{2-} ions. Deionized water was used in solution preparation using molarity formula [13] in Equation 1 and rinsing stages. Glass slides were used as substrates due to the chemical stability of the reagents, and optical clarity. Prior to deposition, the slides were ultrasonically cleaned in a mixture of acetone, ethanol, and deionized water for 10 minutes each and then dried in ambient air to ensure contaminant-free surfaces.

$$Molarity = \frac{Mass\ needed}{MolarMass \times Volume} \quad (1)$$

The SILAR process involved sequential immersion of substrate in cationic (Pb^{2+} or Zn^{2+}) and anionic (S^{2-}) solutions with deionized water rinsing in-between the steps, to remove unadsorbed ions. Each cycle consisted 10 minutes immersion in Pb^{2+}, S^{2-}, Zn^{2+} and S^{2-} solutions each with 5 minutes rinses. Six sets of films were prepared with 4, 6, 8, 10, 12 or 14 cycles. Fresh precursor solutions were prepared before each deposition to ensure consistent ion concentrations.

2.2 Characterization

The synthesized PbS/ZnS thin films were characterized using a range of analytical techniques to assess their structural, morphological, optical, and electrical properties. The thickness of 4, 6, 8, 10, 12, and 14 cycles were determined with Profiler and obtained as 0.90, 0.90, 1.01, 2.70, 3.00, and 3.20 μm respectively.

2.2.1 X-ray diffraction

X-ray diffraction (XRD) Tongda TD-3500 was employed to identify the crystalline structure, phase composition, and estimate crystallite size, utilizing Cu-Kα radiation (λ = 1.5406 Å) within a 2θ scanning range of 20° to 70°. The average crystallite size (D) of PbS films was evaluated through the peak full width at half maximum (FWHM), by implementing the Debye-Scherrer formula:

$$D = \frac{k\lambda}{\beta COS\ \theta} \quad (2)$$

where, 'λ' = 1.5406 Å (Cu-kα wavelength), 'θ' is the Bragg's angle of the peaks, and 'β' is the full width at half maximum (FWHM), 'k' = 0.9 (Shape factor).

2.2.2 Scanning Electron Microscopy

The surface morphology and grain texture were examined using scanning electron microscopy (SEM), EVO/MA 10 model for insight into the film's uniformity and structural features. Elemental analysis was carried out through Energy Dispersive X-ray spectroscopy (EDS), integrated with SEM, to verify the presence and distribution of lead, zinc, and sulphur elements, thereby confirming successful co-deposition.

2.2.3 UV-Visible Spectroscopy

The Optical characteristics were studied using ultraviolet (UV) spectrophotometer (FILMETRICS F10-RT-UV model), over a 200–1100 nm wavelength range. The Tauc plot was achieved using Equation 3 for direct energy bandgap of the co-deposited semiconductors.

$$(\alpha hv)^2 = A(hv - E_g) \quad (3)$$

J. of Science and Technology Vol. 17 No. 2 (2025) p. 166-177

Where: α is the absorption coefficient; $h\nu$ is the photon energy (h is Planck's constant, ν is frequency), A is a constant, and E_g is the bandgap energy.

$$E = hc\lambda = \frac{1240}{\lambda} \tag{4}$$

2.2.4 Hall Effect Measurement

Hall Effect is a method of determining the electrical properties of a semiconductor. The Hall Effect characterization was done using ECOPIA Hall Effect Measurement System, model HMS-3000. A current of 0.01 μA, delay time under the influence by magnetic field 0.535 T, using thickness of 40 μm and measurement number of 1,000 times.

$$V_H = E_H t \tag{5}$$

$$E_H = R_H J_x B_z \tag{6}$$

$$\mu = \frac{R_H J_x}{E_x} \tag{7}$$

$$\mu = \sigma R_H \tag{8}$$

$$\sigma = \frac{1}{\rho} \tag{9}$$

where V_H = hall voltage, t = thickness, $R_H = -\frac{1}{n_e}$, hall coefficient, J_x = current density in the x-direction, B_x = magnetic field strength, n_e = amount of charge, μ = mobility, E_H = hall electric field, E_x = electric field in the x-direction, σ = conductivity, ρ = resistivity.

3. Results and Discussion

The X-ray diffraction patterns of the co-deposited samples on glass substrates at room temperature are shown in Fig. 1. The Miller indices of the peaks can be restricted to two different phases: the cubic phases of PbS and ZnS. The Fig. 1 showed the diffraction peaks at 25.89°, 29.88°, 42.97°, 50.88°, and 57.86° related to (111), (200), (220), (311), and (222) of the cubic phase of PbS with JCPDS 05-0592 respectively. While the peaks at 2θ values at 27.03°, 34.55°, 43.22°, 52.10°, and 66.85° related to reflection at (111), (200), (220), (311) and (222) planes of cubic ZnS with JCPDS of 05-0566 [14]. The synthesized crystals, (like in the case of bulk PbS (galena)) pattern, the peak corresponding to (200) lattice plane is the most intense peak, the intensity of the diffraction peak related to (200) plane in PbS phase is significantly stronger than that of other peaks [15].

Peak intensity and sharpness increased with deposition cycles, indicating improved crystallinity and larger crystallite sizes. The crystallite sizes calculated using Debye-Scherer equation ranged between 3.63 nm and 45.33 nm (Table 1). Smaller crystallite sizes at lower cycles (4 and 6) suggest higher defect densities, while larger sizes at higher cycles (12 to 14) indicates grain growth and reduced strain [16].

Fig. 2 revealed the morphological properties of the co-deposited PbS/ZnS with increasing nucleation as the number of cycle increased. The particles nucleation became significant from cycle 8 (Fig. 2C) to cycle 14 (Fig. 2F). The whitish patches were as a result of particles being charged by electrons from the SEM.

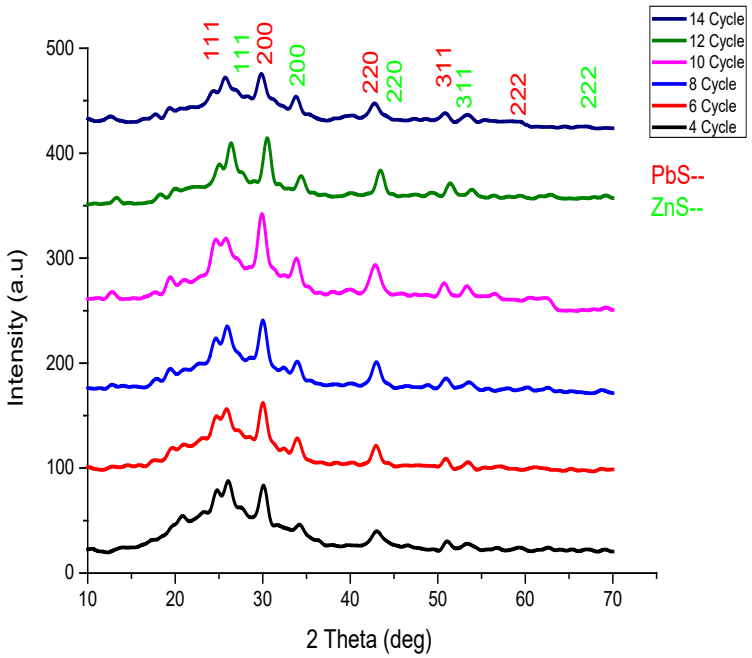

Fig. 1 *XRD spectra of As-synthesized PbS/ZnS thin films*

Table 1 *XRD details of As-synthesized PbS/ZnS thin films*

2θ (°)	d-spacing (nm)	FWHM (rad)	Crystallite Size, D, (nm)	Millar Indices (hkl)	Assigned Phases
25.894	0.343	0.211	6.65	(111)	PbS (cubic)
27.033	0.329	0.067	21.02	(111)	ZnS (cubic)
29.888	0.299	0.341	4.22	(200)	PbS (cubic)
34.550	0.263	0.164	8.99	(200)	ZnS (cubic)
42.979	0.210	0.428	3.63	(220)	PbS (cubic)
43.222	0.205	0.294	5.29	(220)	ZnS (cubic)
50.888	0.179	0.149	10.85	(311)	PbS (cubic)
52.105	0.175	0.034	45.33	(311)	ZnS (cubic)
57.868	0.159	0.090	17.64	(222)	PbS (cubic)
66.857	0.139	0.133	12.60	(400)	ZnS (cubic)

J. of Science and Technology Vol. 17 No. 2 (2025) p. 166-177

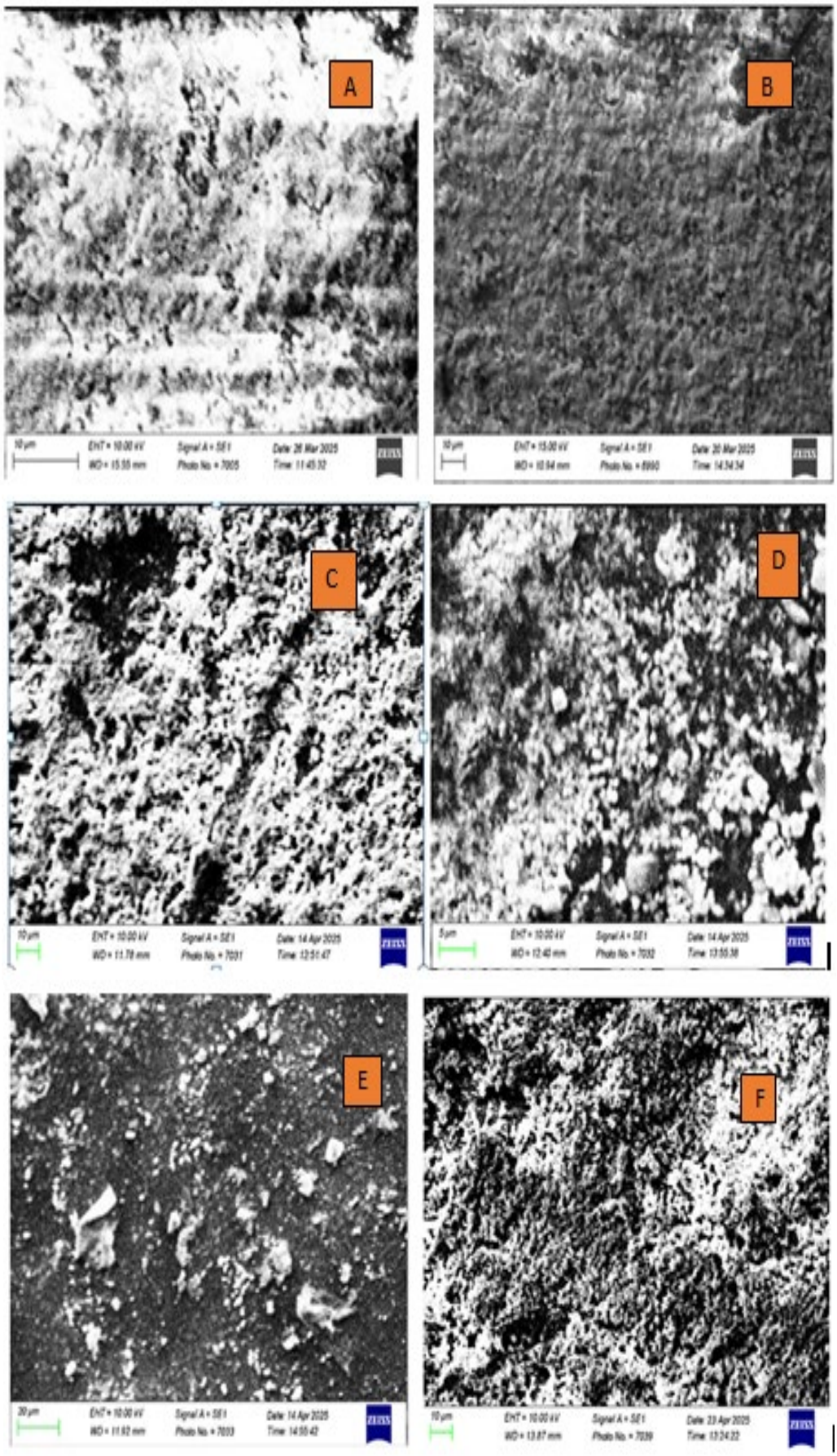

Fig. 2 *SEM images of PbS/ZnS thin films (a) 4-cycles; (b) 6-cycles; (c) 8-cycles; (d) 10-cycles; (e) 12-cycles; (f) 14 cycles*

In Fig. 3, the EDS confirmed the presence of lead, zinc, and sulphur in the deposited samples, with lead dominating the spectrum, indicating PbS as the primary phase. Zinc is also present, albeit with weaker signals, suggesting a secondary ZnS phase dispersed throughout the film [17]. The EDS show the composition of PbS/ZnS thin films changes significantly with increasing SILAR cycles. The Zn content increases steadily from 4 to 12 cycles (6.22% to 25.25%). This indicated a successful incorporation of ZnS into PbS [11, 15]. In contrast, the Pb content is highest at 4-6 cycles (>50%), reflecting a PbS-dominant structure initially, but drops significantly by 12 cycles (~38%) as ZnS coating increases [4, 18]. The sulphur content remains relatively stable up to 10 cycles but decreases at higher cycles, due to sulphur loss and surface effects [12]. The PbS/ZnS ratio becomes more balanced around 12 cycles, suggesting an optimal co-deposition balance. The EDS data in Table 2, confirmed the successful incorporation of ZnS into the PbS matrix, with 12 cycles yielding a more balanced composition of Zn, S, and Pb [17, 19]. This balance is ideal for optimizing optoelectronic properties.

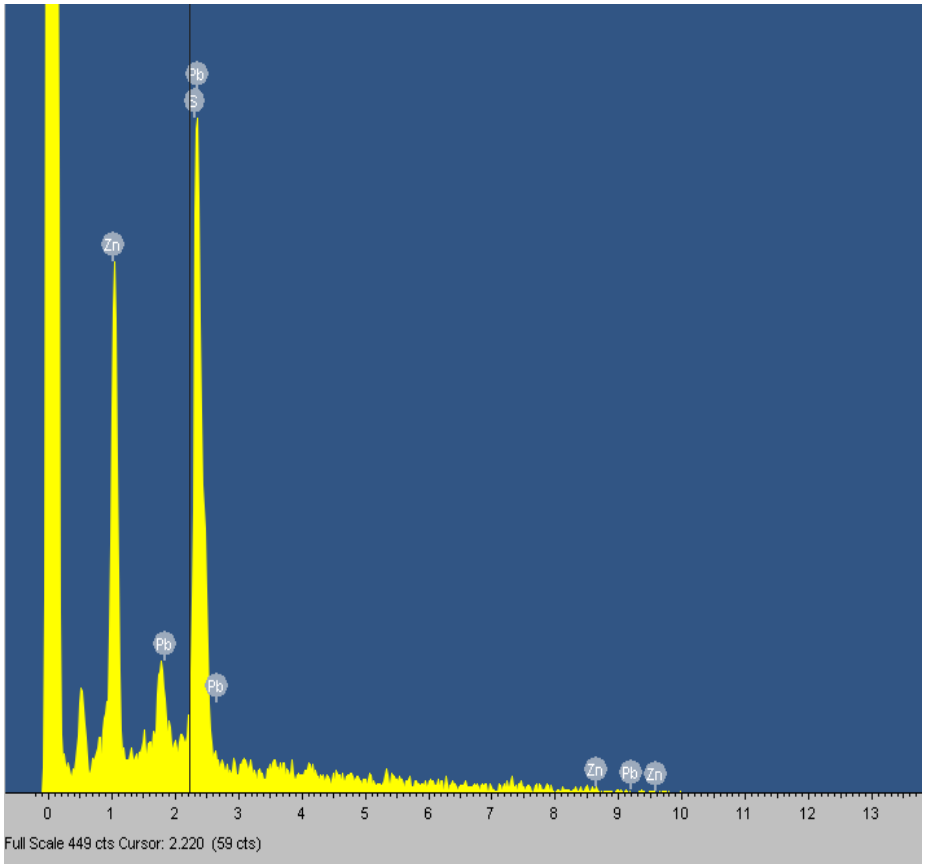

Fig. 3 *EDS spectra of As-synthesized PbS/ZnS nanoparticle deposited on glass substrate*

J. of Science and Technology Vol. 17 No. 2 (2025) p. 166-177

Table 2 *EDS percentage composition of as-synthesized PbS/ZnS nanoparticles*

Samples	Elements	Weight (%)	Atomic (%)
4 cycles	Zn	3.23 +/-0.45	6.22
	S	10.54 +/0.57	41.39
	Pb	86.23 +/-0.70	52.40
	Total	100.00	100.00
6 cycles	Zn	1.99 +/-0.34	3.73
	S	11.92. +/0.50	45.56
	Pb	86.09 +/-0.68	50.81
	Total	100.00	100.00
8 cycles	Zn	7.39 +/-0.60	13.25
	S	11.14 +/0.71	40.70
	Pb	81.47 +/-0.90	46.06
	Total	100.00	100.00
10 cycles	Zn	5.16 +/-0.68	9.58
	S	10.90 +/0.85	41.25
	Pb	83.94 +/-1.05	49.17
	Total	100.00	100.00
12 cycles	Zn	22.69 +/-1.40	25.25
	S	7.41 +/0.94	36.85
	Pb	69.90 +/-1.57	37.90
	Total	100.00	100.00
14 cycles	Zn	13.40 +/-0.62	25.24
	S	6.41 +/0.52	25.89
	Pb	80.19 +/-0.76	48.87
	Total	100.00	100.00

Fig. 4 showed the absorbance spectra of PbS/ZnS thin films with varying cycle numbers (4 to 14 cycles). It revealed the absorbance increase with cycle number, particularly in the UV region [20-22]. In the visible to near-infrared region, the absorbance spectra exhibit distinct behaviors, with 4 and 6 cycles displaying lower absorbance while higher cycle numbers 8-14 cycles, showing stronger and more stable absorbance across a broad wavelength range 200-1150 nm. The increase in the absorbance with the number of cycles in the UV region is attributed to the increase in film thickness, which enhanced light absorption [17]. Notably, films with 8 to 14 cycles exhibited stable and high absorbance, making them suitable for optoelectronic applications like photodetectors or solar cells [23-25]. The absorbance trends also correlate with earlier-provided thickness data, confirming consistent growth with SILAR cycles [4, 17].

Fig. 5 showed the decrease in transmittance with increase in deposition cycle, ranging from ~3.5% for 4 cycles to near-zero for 14 cycles, due to the formation of denser and thicker films that obstruct light [17, 19]. In the UV region ranging (200 to 400 nm), all films exhibited low transmittance, indicating strong absorption, while in the visible to near-NIR region 400 to 1200 nm, only the thinner films 4 to 6 cycles showed notable transmittance. The decrease in transmittance with increasing cycles is attributed to the increased optical density and thickness of the films, making them suitable for applications requiring strong light absorption, such as absorber layers in solar cells and photodetectors. In contrast, films with fewer cycles and higher transmittance may be suitable for window layers or transparent electrodes, highlighting the tunable optical properties of these materials via deposition cycles [4,17,19].

In Fig. 6, the increase in cycle number exhibit a notable decline in reflectance, signifying enhanced light absorption capabilities [17, 19, 26]. Films with 10-14 cycles displayed exceptionally low reflectance, often to achieve antireflective coatings and making them well-suited for optoelectronic devices like solar cells [17, 19, 27]. The correlation between cycle number and reduced reflectance underscores the film's densification and improved light-harvesting properties [19, 27]. Specifically, 12 and 14 cycle films showed optimal performance, balancing high absorption with minimal reflectance. Any negative reflectance readings at higher cycles likely stem from measurement anomalies rather than inherent material properties [15,19].

In Fig. 7, the Tauc plots for PbS/ZnS thin films with varying SILAR cycles showed that, the bandgap energy increased with the number of cycles, from 1.43 eV for 4 and 6 cycles, to 2.82 eV for 14 cycles. The shift towards higher bandgap energies with increasing cycles implies a reduction in quantum confinement effects as the film

thickness grows. The wide variation of the wavelength/frequency were noted thus, correlated plots were done for proper evaluation if bandgaps. Additionally, the improvement in crystallinity and stoichiometry with more cycles also contributed to the observed bandgap shift, highlighting the complex interplay between film thickness, structure, and optical properties [19, 28].

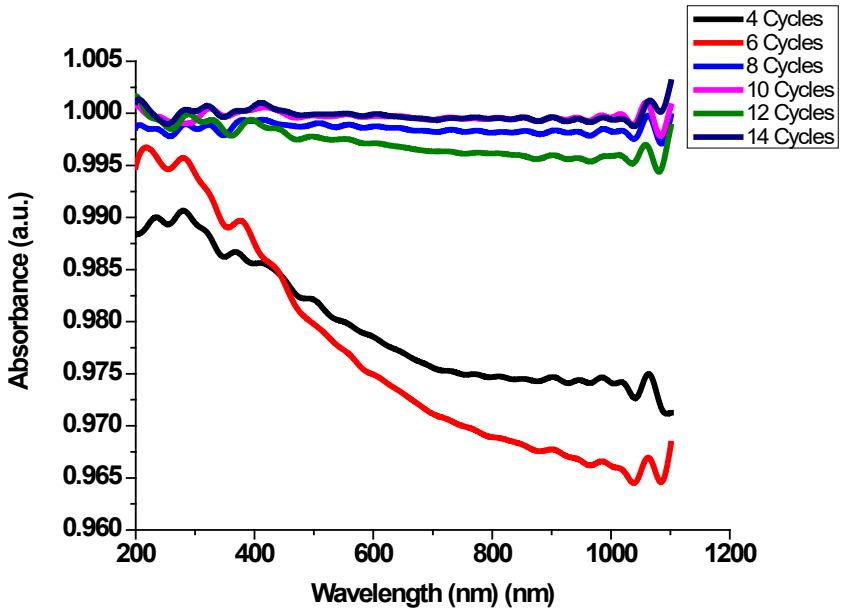

Fig. 4 *Absorbance spectra of PbS/ZnS thin films*

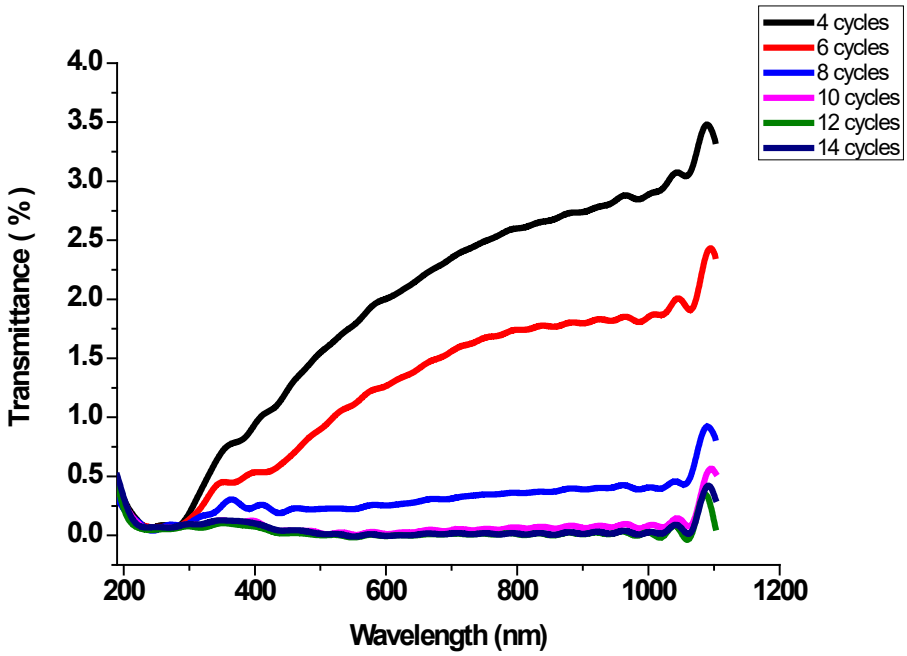

Fig. 5 *Transmittance spectra of PbS/ZnS thin films*

J. of Science and Technology Vol. 17 No. 2 (2025) p. 166-177

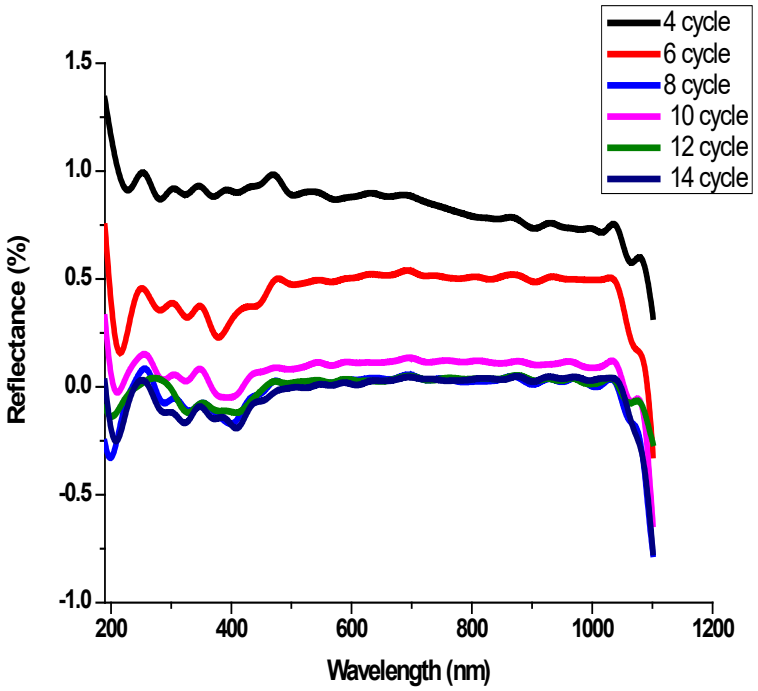

Fig. 6 *Reflectance spectra of PbS/ZnS thin films*

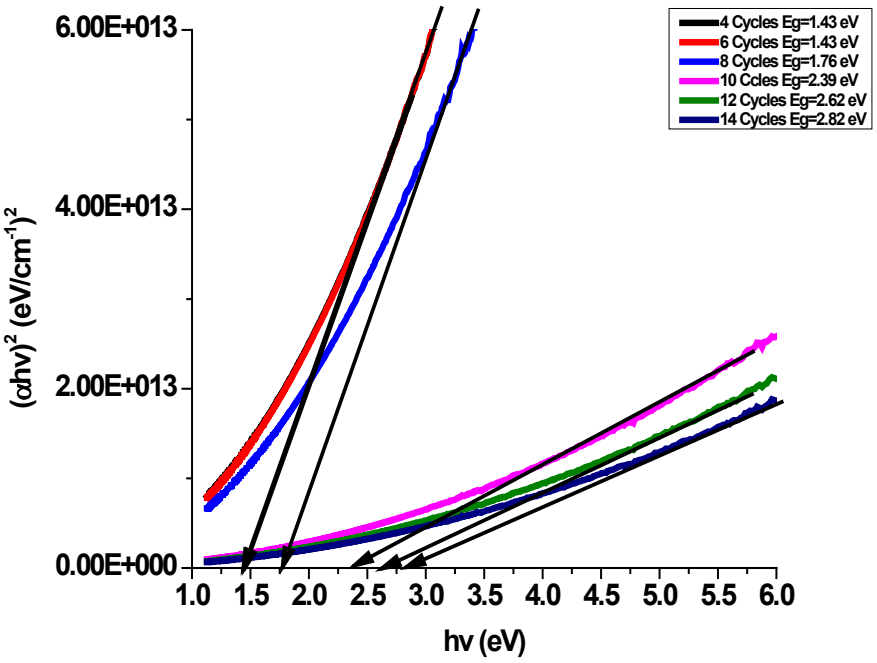

Fig. 7 *Tauc plot for optical bandgap of PbS/ZnS thin films*

Hall Effect measurements in Table 3 reveal n-type conductivity for all the films, with bulk carrier concentration decreasing from $1.616 \times 10^{12} cm^{-3}$ (4 cycles) to $1.476 \times 10^{11} cm^{-3}$ (14 cycles). Carrier mobility peaks at $5.482 \times 10^{2} cm^{2}/Vs$ for 8 cycles suggesting reduced grain boundary scattering due to improved microstructure. Resistivity increases with cycles reaching $1.054 \times 10^{5} \Omega cm$ at 14 cycles indicating lower carrier densities and increased trap rate [19, 28].

Table 3 *Hall effect table for different deposition samples*

Deposition cycles	Bulk concentration (cm^{-3})	Mobility (cm^2/Vs)	Resistivity (Ω cm)	Conductivity (S/cm)	Hall Coefficient (cm^3/C)	Carrier Type
4	$-1.616x10^{12}$	$1.107x10^{2}$	$3.487x10^{4}$	$2.868x10^{-5}$	$-3.862x10^{6}$	n-type
6	$-4.841x10^{12}$	$1.308x10^{2}$	$9.918x10^{3}$	$1.008x10^{-4}$	$-1.297x10^{6}$	n-type
8	$-4.076x10^{11}$	$5.482x10^{2}$	$2.794x10^{4}$	$3.597x10^{-5}$	$-1.532x10^{7}$	n-type
10	$-4.449x10^{11}$	$1.566x10^{2}$	$8.962x10^{4}$	$1.116x10^{-5}$	$-1.400x10^{7}$	n-type
12	$-3.810x10^{11}$	$1.594x10^{2}$	$1.028x10^{5}$	$9.730x10^{-6}$	$-1.638x10^{7}$	n-type
14	$-1.476x10^{11}$	$4.015x10^{2}$	$1.054x10^{5}$	$9.492x10^{-6}$	$-4.230x10^{7}$	n-type

4. Conclusion

PbS/ZnS thin films were synthesized via the SILAR method, with a cubic structure and reflections from specific planes. The broadening of diffraction peaks provided insight into crystallite size. Optical studies revealed that these films possess good optical properties, with low transmittance in the UV region (200-400 nm) due to strong absorbance and notable transmittance in the visible to NIR region (400-1200 nm) for thinner cycles. The optical properties can be tailored by adjusting deposition cycles, making higher cycles suitable for absorber layers and photodetectors, while lower cycles are suitable for window layers and transparent electrodes. The bandgaps ranged from 1.43 to 2.82 eV, rendering PbS/ZnS thin films suitable for optoelectronic and photovoltaic applications due to their tunable bandgap properties. Surface morphology analysis showed uniform coverage with increasing grain size corresponding to more deposition cycles. EDS confirmed the presence of lead, zinc, and sulphur in the films. Hall Effect measurements indicated n-type conductivity, with electrical properties influenced by SILAR deposition cycles. Optimal properties were achieved at 4, 6 and 8 cycles, suggesting PbS/ZnS films as promising materials for window layers in optoelectronic applications. However, surface roughness and non-uniformity at higher cycles may limit device performance, warranting further optimization of deposition parameters.

Acknowledgement

The authors acknowledged the technical assistance from the technical department.

Conflict of Interest

The authors declare that there is no conflict of interest regarding the publication of the paper.

Author Contribution

The authors confirm contribution to the paper as follows: ***study conception and design:*** *Olayinka A. Babalola, Ibrahim B. Omotej;i* ***data collection:*** *Francis O. Omoniyi, Ibrahim B. Omoteji;* ***analysis and interpretation of results:*** *Francis O. Omoniyi, Ibrahim B. Omoteji, Olayinka Babalola, Thomas I. Imalerio;* ***draft manuscript preparation:*** *Francis O. Omoniyi, Ibrahim B. Omoteji, Olayinka Babalola. All authors reviewed the results and approved the final version of the manuscript.*

References

[1] Shakil, M. A., Das, S., Rahman, M. A., Akther, U. S., Majumdar, M. K., & Rahman, M. K. (2018). A review on zinc sulphide thin film fabrication for various applications based on doping elements. *Materials Sciences and Applications, 9*(9), 751–778. https://doi.org/10.4236/msa.2018.99055.

[2] Fang, X. S., Zhai, T. Y., Gautam, U. K., Li, L., Wu, L., Bando, Y., & Golberg, D. (2011). ZnS nanostructures: From synthesis to applications. *Progress in Materials Science, 56*(2), 175–287. https://doi.org/10.1016/j.pmatsci.2010.10.001.

[3] Chattarki, A. N., Kamble, S. S., & Deshmukh, L. P. (2012). Role of pH in aqueous alkaline chemical bath deposition of lead sulphide thin films. *Materials Letters, 67*(1), 39–41. https://doi.org/10.1016/j.matlet.2011.09.079.

[4] Ubale, U. Y., Belwalkar, A. N., & Rane, R. Y. (2020). Synthesis and characterization of nanocrystalline PbS thin films by chemical bath deposition method. *Journal of Materials Science: Materials in Electronics, 31*(16), 11513–11523. https://doi.org/10.1007/s10854-020-03759-9.

[5] Goudarzi, A., Aval, G. M., Sahraei, R., & Ahmadpoor, H. (2017). Ammonia-free chemical bath deposition of nanocrystalline ZnS thin film buffer layer for solar cells. *Thin Solid Films, 624*, 14–22. https://doi.org/10.1016/j.tsf.2016.12.035.

[6] Londoño-Monsalve, J., Calderón, J. A., & Devia, A. (2020). Synthesis of PbS thin films by the spray pyrolysis method. *Journal of Physics: Conference Series, 1708*(1), 012005. https://doi.org/10.1088/1742-6596/1708/1/012005.

[7] Eze, C. B., Ezenwa, I. A., Okoli, N. L., Elekalachi, C. I., & Okereke, N. A. (2023). Study of Optical and Structural Properties of SILAR-deposited Cobalt Sulphide Thin Films. *Journal of Nano and Materials Science Research*, *2*(1), 123–130.

[8] Ratnayake, S. P., Ren, J., Colusso, E., Guglielmi, M., Martucci, A., & Della Gaspera, E. (2021). SILAR deposition of metal oxide nanostructured films. *Small, 17*(44), 2101666. https://doi.org/10.1002/smll.202101666.

[9] Lin, J., Kilani, M., Baharfar, M., & Mao, G. (2024). Understanding the nanoscale phenomena of nucleation and crystal growth in electrodeposition. *RSC*, 16, 19564-19588.

[10] Zhu, H., Zhang, W., Zhao, K., Jin, C., Zhang, Z., Xu, K., Liu, Y., Wang, J., &Saetang, V. (2025). Recent advances in precision deposition techniques on semiconductors surfaces: Mechanism, methods, and applications, *Materials Today Communication*, 48, 113495.

[11] Deshpande, N. G., Gudage, Y. G., Sharma, R., Vyas, J. C., Kim, J. B., & Lee, Y. P. (2009). Studies on nanocrystalline lead sulphide (PbS) thin films deposited by successive ionic layer adsorption and reaction (SILAR) method. *Sensors and Actuators B: Chemical, 138*(1), 76–84. https://doi.org/10.1016/j.snb.2009.01.028.

[12] Goudarzi, A., Aval, G. M., Sahraei, R., & Ahmadpoor, H. (2008). Ammonia-free chemical bath deposition of nanocrystalline ZnS thin film buffer layer for solar cells. *Thin Solid Films, 516*(15), 4953–4957. https://doi.org/10.1016/j.tsf.2008.02.013.

[13] Brown, T. L., LeMay, H. E., Bursten, B. E., Murphy, C., & Woodward, P. (2018). *Chemistry: The Central Science* (14th Ed.). Pearson.

[14] Parmar, D. M. (2016). Structural analysis of PbS synthesized by different technique. *International Journal for Innovative Research in Multidisciplinary Field, 2*(7), 2455–0620.

[15] Ubale, A. U., & Belkhedkar, M. R. (2016). Synthesis and characterization of nanostructured PbS thin films by chemical route. *Journal of Materials Science: Materials in Electronics, 27*(6), 6613–6619. https://doi.org/10.1007/s10854-016-4514-4.

[16] Gubicza, J. (2022). Reliability and interpretation of the microstructural parameters determined by x-ray line profile analysis for nanostructured materials. *European Physical Journal Special Topics, 231*(23–24), 4153–4165. https://doi.org/10.1140/epjs/s11734-022-00572-z.

[17] Kumar, P., Singh, A., & Sharma, R. (2018). Impact of deposition cycles on the properties of ZnS thin films. *Journal of Materials Science: Materials in Electronics, 29*(10), 8424–8431. https://doi.org/10.1007/s10854-018-8854-5.

[18] Patil, S. I., Bagade, A. A., & Deshmukh, M. P. (2017). Effect of deposition cycles on the properties of CdS thin films. *Journal of Alloys and Compounds, 725*, 362–369. https://doi.org/10.1016/j.jallcom.2017.05.156.

[19] Patil, R. A., Ma, Y. R., & Patil, P. S. (2016). Synthesis and characterization of PbS thin films. *Journal of Materials Science, 51*(11), 5454–5463. https://doi.org/10.1007/s10853-016-9864-4.

[20] Sundhar, A. (2022). Development of ZnS thin film with Co, Cu and Ag doping using SILAR method. *Materials Today: Proceedings, 48*, 377–381. https://doi.org/10.1016/j.matpr.2021.12.377.

[21] Kumar, G., Balaji, P., Gnana, P., Kaushik, R., & Shriram, M. (2021). Investigations on SILAR coated CZTS thin films for solar cells applications. *Phase Transitions, 94*(6), 556–566. https://doi.org/10.1080/01411594.2021.1945677.

[22] Geethanjali, M. T., Depa, K., & Remadevi, T. (2021). Effect of number of cycles on SILAR deposited ZnSe thin films. *AIP Conference Proceedings, 2395*, 060009. https://doi.org/10.1063/5.0067963.

[23] Lim, J. W., Wang, H., Choi, C. H., Kwon, H., Quan, L. N., Park, W.-T., Noh, Y.-Y., & Kim, D. H. (2019). Self-powered reduced-dimensionality perovskite photodiodes with controlled crystalline phase and improved stability. *Nano Energy, 57*, 761–770. https://doi.org/10.1016/j.nanoen.2019.04.064.

[24] Xie, C., Liu, C. K., Loi, H. L., & Yan, F. (2020). Perovskite-based phototransistors and hybrid photodetectors. *Advanced Functional Materials, 30*(19), 1903907. https://doi.org/10.1002/adfm.201903907.

[25] Zhao, K., & Zhu, K. (2016). Organic–inorganic hybrid lead halide perovskites for optoelectronic and electronic applications. *Chemical Society Reviews, 45*(3), 655–689. https://doi.org/10.1039/C4CS00458B.

[26] Savadkoha, M., & Bagheri-Mohagheghi, M. M. (2020). Effect of deposition cycles on the optical properties of CdS thin films prepared by SILAR method. *Journal of Materials Science: Materials in Electronics, 31*(12), 9743–9752. https://doi.org/10.1007/s10854-020-03564-4.

[27] Goudarzi, M., & Salavati-Niasari, M. (2020). Effect of deposition cycles on the optical properties of CdS thin films prepared by SILAR method. *Journal of Materials Science: Materials in Electronics, 31*(2), 1423–1432. https://doi.org/10.1007/s10854-019-02657-4.

[28] Shrivastava, A., Dubey, A., & Singh, R. K. (2021). Impact of deposition cycles on the electrical properties of nanostructured thin films. *Journal of Materials Science: Materials in Electronics, 32*(5), 5713–5723. https://doi.org/10.1007/s10854-021-05457-6.